Supplementary material of the article

Search for the optimal design of a supercritical-CO_2 Brayton power cycle from a superstructure-based approach implemented in a commercial simulation software

Qiao Zhao[1,2], Mounir Mecheri[2], Thibaut Neveux[2],
Romain Privat[1], Jean-Noël Jaubert[1], Yann Le Moullec[2]

[1] Université de Lorraine, École Nationale Supérieure des Industries Chimiques,
Laboratoire Réactions et Génie des Procédés (UMR CNRS 7274),
1 rue Grandville, 54000 Nancy, France,
[2] EDF R&D Chatou, 6 quai Watier, 78400 Chatou, France.

1 Validation of the proposed approach using a simplified superstructure

1.1 Definition of a simplified superstructure for approach validation

In order to validate the proposed approach, we decided to first consider a simplified superstructure encompassing a limited number of different Brayton cycle layouts and among these, a well-identified optimal cycle. The simplified superstructure used in this study was generated by integrating the various Brayton cycles (cases 1 to 3) presented in Figure 8 of reference [1] in a unique master process described in Figure S1).

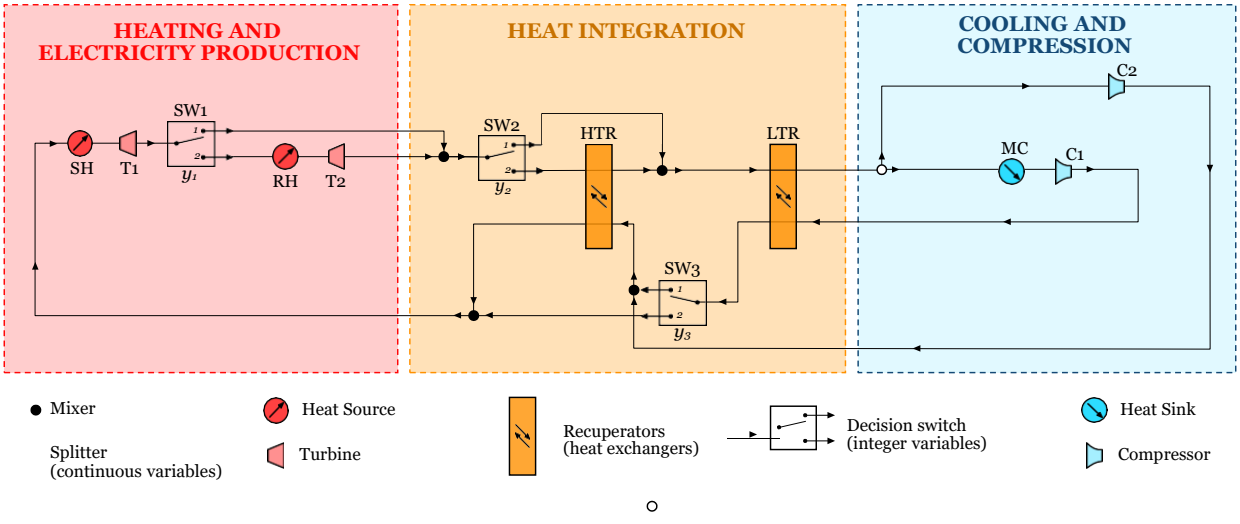

Figure S1: Example of the superstructure of a S-CO_2 Brayton cycle ($2^3 = 8$ structural alternatives). Units *H*(*orL*)*TR* are recuperators (heat exchangers for thermal integration), *T* are turbines, and *C* are compressors.

The proposed superstructure is composed of three different blocks: the heat source and electricity-production block, the heat-integration block, and the cooling and compression block. From left to right,

- The first logical switch *SW1* makes it possible to activate a reheating stage (and then switch from one to two turbines).
- The second flow switch, *SW2*, enables the last turbine's outlet stream to cross or bypass the extra heat recuperator, HTR.
- The third flow switch, *SW3*, decides whether the compressor C2 outlet goes straightforwardly to the heat-source exchanger or is preheated first in the extra recuperator HTR.

Due to the presence of three decision flow switches, this superstructure enables $2^3 = 8$ different layouts. Among these, two are redundant, and consequently, the superstructure contains actually six distinct S-CO_2 Brayton cycles. According to reference [1], the Brayton cycle layout with the reheating stage and thehighest thermal integration degree (i.e., with *SW2* directing the last turbine's outlet stream to HTR and *SW3* directing the compressor C1 outlet to HTR) is expected to be the most efficient one.

1.2 List of the optimized variables and specification equations

The design of the S-CO_2 Brayton cycle from the simplified superstructure, presented in Figure 2 of the article, requires the determination of 10 continuous and integer variables (*optimized variables*) enumerated in Table S1, which are temperatures, pressures, recycle flow rate ratio and flow-switch decision variables.

The bounds of variables were based on state-of-the-art ultra-supercritical steam (USC-steam) Rankine cycle conditions (30 MPa, 893.15 K). Table S1 provides the modeling equipment data and assumptions such as isentropic efficiencies of turbo-machineries, minimal pinch temperature, and assumed pressure drops.

Note that the *final* turbine T2 and compressor C2 outlet pressures depend on the cycle layout and thus can be deduced from other optimized variable values (and, in particular, integer variables). Logical rules were applied in the simulation block to determine their values: the C2 outlet pressure was set equal to the pressure of the other inlet stream of the mixer, while the T2 outlet pressure was determined as explained in Section 2.5 of the article.

1.3 First validation step: solving the Non-linear Problem for a fixed cycle layout

As the first validation step, we decided to test the capacity of the developed tool to solve a simpler problem than the MINLP, i.e., an NLP (Non-Linear Problem). To do so, the simplified superstructure defined above was used, but integer variables (of flow switch units) were fixed, which is equivalent to the specification of a particular cycle layout. The optimization problem was thus reduced to the determination of the seven real variables $\mathbf{x}$ (defined in Table S1). Six different cycle layouts were considered by combining the two possible values (1 or 2) of the three switch variables (denoted y_1, y_2, and y_3). Itis recalled that although $2^3 = 8$ cycle layouts could be defined from these combinations, two of them are redundant, explaining why only six layouts were finally considered. These cycles are represented in Figure S2; the values of the $\{ y_1, y_2, y_3 \}$ variable sets associated with each layout are mentioned belowthe cycle flowsheet. In each case, the NLP problem was solved, i.e., the values of real variables $\mathbf{x}$ were searched in order to minimize the objective function introduced in Eq. (4) of the article by keeping constant integer variables $\mathbf{y}$, using the MIDACO solver. The results are reported in Table S2.

Table S2 reports cycle efficiencies (i.e., the absolute value of the objective function), optimized variables, constraints, and corresponding cycle parameters for each layout. As expected, the configuration $\{2, 2, 1\}$ is indeed the best one with respect to the fixed objective. By comparing the left column's (without reheating) and the right column's layouts (including reheating) in Figure S2, it can be noticed that the introduction of reheating helps to raise the efficiency by 1.3%-pt as qualitatively expected. Regardless of the considered layout, the optimal cooling temperature ($T_{cooling}$) systematically reaches its lower-bound value ($x_2 = 304.35$ K). In the same way, the compressor outlet pressure, which imposes the value of the turbine inlet pressure (these two pressures are about the same), always reaches its upper

Table S 1: List of the 10 optimized variables, their corresponding bounds, the values of fixed process variables, equipment data and constraints used in the superstructure

Optimized continuous variables x	**Bounds**
Compressor Inlet Pressure P_{in} (MPa)	$x_1 \in 3.3 - 10$ CO_2
Cooling Temperature $T_{cooling}$ (K)	$x_2 \in 304.35 - 373.15$
CO_2 Mass Flow Ratio between Recompression Stream and Main Stream (%)	$x_3 \in 10^{-6} - 0.5$
Compressor Outlet Pressure P_{out} (MPa)	$x_4 \in 3.3 - 30$
LTR Cold Stream Outlet Temperature T_{LTR} (K)	$x_5 \in 304.35 - 893.15$
Turbine (T1) Expansion Ratio = P_{in}/P_{out} (-)	$x_6 \in 1 - 5$ HTR
Hot Stream Outlet Temperature T_{HTR} (K)	$x_7 \in 304.35 - 893.15$
Optimized integer variables y	**Bounds**
Switch *SW1* (integer variable)	$y_1 \in \{1, 2\}$
Switch *SW2* (integer variable)	$y_2 \in \{1, 2\}$
Switch *SW3* (integer variable)	$y_3 \in \{1, 2\}$
Variable specifications and equipment data	**Value**
Main Turbine Inlet Temperature T_{it1} (K)	893.15
Secondary Turbine Inlet Temperature (after reheating) T_{it2} (K)	893.15
CO_2 Flowrate in Main Cooling (kg/s)	6 000
Minimal Recuperators (LTR and HTR) Temperature Pinch ΔT_{pinch} (K)	10
Turbine Isentropic Efficiency η_{Tis} (-)	0.90
Compressor Isentropic Efficiency η_{Cis} (-)	0.89
Pressure Drop in every component Δ_P (in % of Inlet Pressure)	1%
Constraints	**Definition**
g_1 on LTR Cold End Temperature Difference (K)	$(\Delta T - \Delta T_{pinch}) \geqq 0$
g_2 on LTR Hot End Temperature Difference (K)	$(\Delta T - \Delta T_{pinch}) \geqq 0$
g_3 on HTR Hot End Temperature Difference (K)	$(\Delta T - \Delta T_{pinch}) \geqq 0$
g_4 on HTR Cold End Temperature difference(K)	$(\Delta T - \Delta T_{pinch}) \geqq 0$
g_5 on Pressure Ratio of the Main Compressor C1 (-)	$(P_{out}/P_{in} - 1) \geq 0$

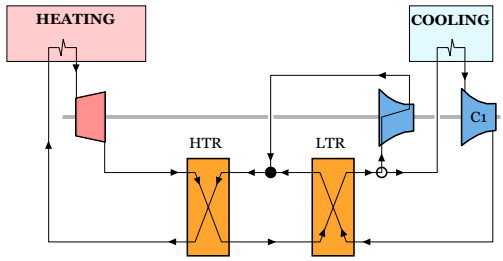

(a) Case y = {1;2;1}

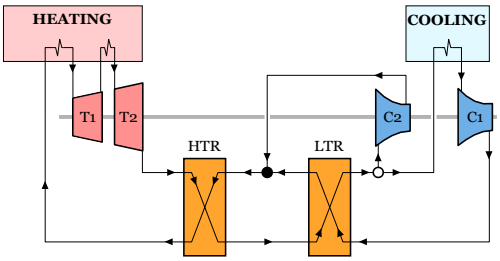

(b) Case y = {2;2;1}

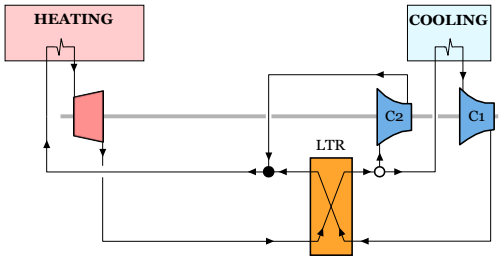

(c) Case y = {1;1;(1 or 2)}

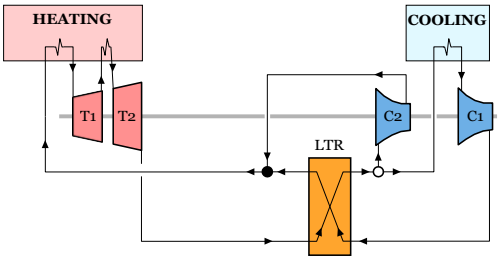

(d) Case y = {2;1;(1 or 2)}

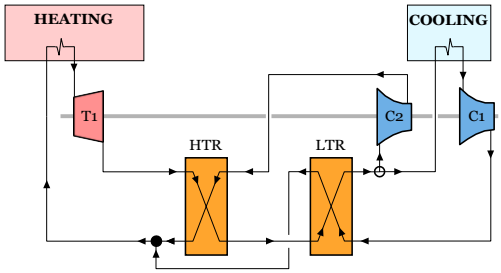

(e) Case y = {1;2;2}

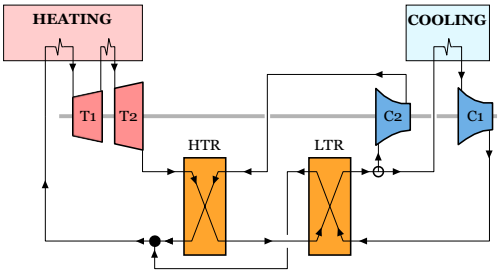

(f) Case y = {2;2;2}

Figure S2: Description of 6 Brayton cycle layouts generated from the simplified superstructure.

Table S2: Resolution of NLP: optimization results for six Brayton cycle layouts using MIDACO.

Configuration	{1, 2, 1}	{2, 2, 1}	{1, 1, (1or2)}	{2, 1, (1or2)}	{1, 2, 2}	{2, 2, 2}
Net Cycle efficiency (%)	**49.55**	**51.33**	**47.39**	**48.63**	**47.61**	**48.90**
Compressor P_{in} (MPa): x_1	7.61	7.46	7.47	7.44	7.48	7.49
$T_{cooling}$ (K): x_2	304.35	304.35	304.35	304.35	304.35	304.35
Recompression flow ratio (%): x_3	0.34	0.34	0.25	0.20	0.25	0.23
Compressor P_{out} (MPa): x_4	30	30	30	30	30	30
LTR Cold stream Temperature outlet (K): x_5	488.34	497,76	717.04	795.89	660.60	707.16
Main Turbine Expansion ratio (-): x_6	-	1.91	-	1.91	-	1.65
HTR Hot stream Temperature outlet (K): x_7	498.09	507.39	-	-	670.29	716.74
Constraints (tolerance of 0.5 for g_1 to g_5)						
LTR cold end ΔT: g_1 (K)	-0.50	-0.41	-0.41	-0.49	-0.38	-0.45
LTR hot end ΔT: g_2 (K)	-0.25	-0.37	-0.49	-0.49	-0.31	-0.42
HTR hot end ΔT: g_3 (K)	32.02	33,84	-	-	18.38	0.25
HTR cold end ΔT: g_4 (K)	0.02	-0,42	-	-	163.74	210.23
Compression ratio C1: g_5 (-)	58.83	60,44	60,29	60,60	60.20	60.15
Other process variables						
Main turbine Pressure outlet (MPa)	7.84	-	7.62	-	7.71	-
Secondary turbine Pressure outlet (MPa)	-	7.69	-	7.59	-	7.71
Hot stream Temperature outlet (K)	354.80	360.67	359.69	361.66	359.09	359.12
Cold stream Temperature outlet (K)	688.77	763.73	-	-	699.27	778.43
CO_2 Flow Rate in boiler (kg/s)	9208.78	9206.14	7903.31	7643.94	8132.55	7937.07

bound (x_4 = 30 MPa); these results seem obvious, as it is well known that (i) the mechanical work and thus the cycle efficiency increase with the pressure ratio in the turbine, and (ii) the lower the compressor inlet temperature, the lower the compression work. Apart from the cooler temperature and compressor outlet pressure, the other optimized variables, such as the flow to recompression (x_3) and recuperator temperatures, vary from one cycle layout to another one.

Note that a large range of main compressor inlet pressure (x_1) values were considered in this study, and in particular, the lower bound of this variable is lower than the critical CO_2 pressure. In return, the results reported in Table S2 indicate that optimal inlet pressures of C1 are always found around the critical pressure of CO_2 (7.4 MPa).

To conclude, this first study highlights the efficiency of the developed tool for finding the optimal values of real parameters of a fixed Brayton cycle layout.

1.4 Second validation step: solving an MINLP

Introducing integer variables y_i into the optimization problem, the MIDACO routine is run to identify the best layout from the superstructure of Figure S1. Figure S3 gives an overview of the progress- sion of the optimization process in the (η_{cycle} vs. iteration number) plane: the single points correspondto each individual set of integer and real parameters generated during the evolutionary process (i.e., each set corresponds to a given ant colony (AC)); the bold line connects the best elements at each iteration, and, as expected, increases with the number of iterations. Looking at this graph in more detail, it is observed that during the first 1500 iterations, the process converges to a cycle efficiencyaround 50%; by introducing new AC from iteration 1500 onwards (approximately), the MIDACO rou- tine activates a new search space, allowing it to slightly increase the cycle efficiency. A similar trend can be observed around iterations 4000 and 6000.

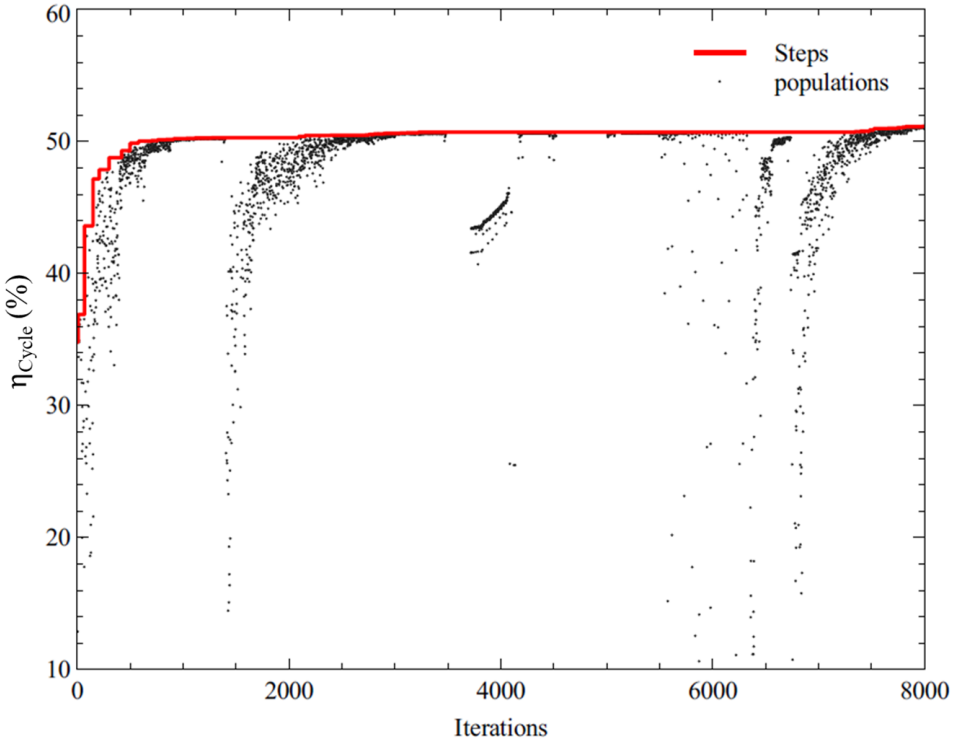

Figure S3: Optimization progress of S-CO_2 Brayton cycle

In the MIDACO routine, the definition of an initial AC is controlled by a pseudo-random-number generator using an initial seed that has to be initialized. By modifying the seed value, differentinitial AC can be generated. To provide an insight into how the selection of an initial AC influencesthe convergence, four optimization processes, all characterized by different initial populations, were run. The result of this test is shown in Figure S4 and highlights that after 160 000 iterations, all processes converge to similar cycle efficiencies. For a deeper analysis, the detailed results are reported in Table S3. Firstly, it is observed that all processes led to the same integer variable set and thus the same optimal Brayton cycle layout. Secondly, it appears that the sets of real variables x_i at convergence are rather independent of the initial guesses. The main difference lies essentially in the optimization process kinetics: some seeds make it possible to evolve more quickly towards optimal solutions than some others. To increase the probability of finding the global solution after a fixed number of iterations, it is thus advised to run different optimization processes, all characterized by different initial seeds.

Assuming now that the solution found by MIDACO is optimal, the obtained result can be com pared with results from the literature. The optimal cycle obtained here is composed of two compressors, tworecuperators, two turbines, and one reheater (see Figure S5); it reaches a cycle efficiency as high as

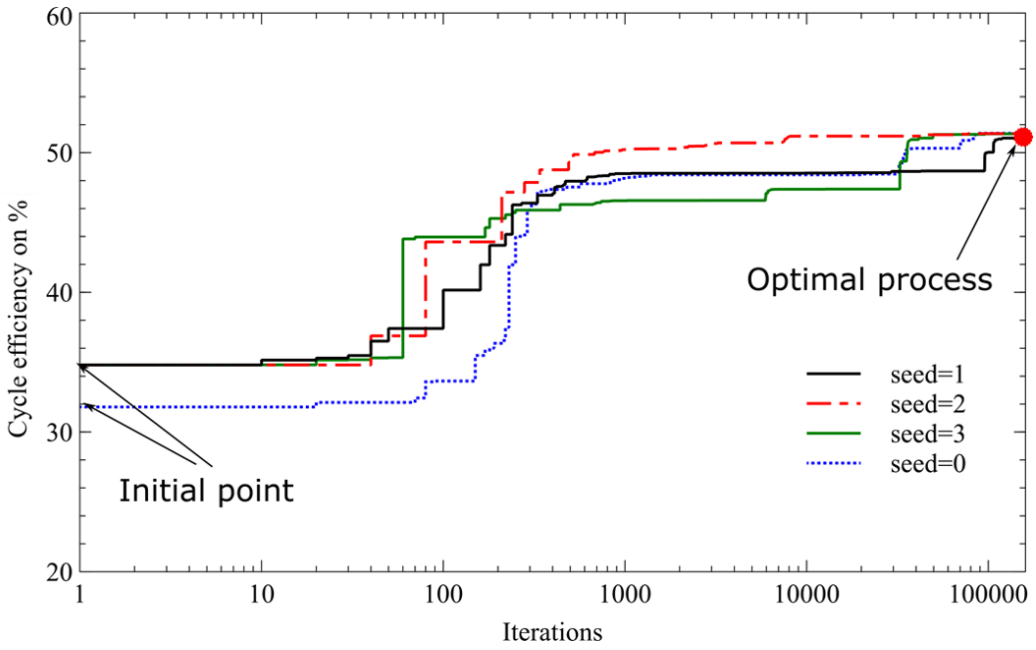

Figure S4: Optimization progress of four runs with different random seeds.

51.4%. Compared with the initial proposal of the S-CO_2 Brayton cycle by Feher and Angelino, [2, 3], the optimal process configuration is improved in terms of heat integration. According to Table S3, all heat exchangers indeed reached the minimal authorized value of the minimal temperature difference ΔT between their hot and cold sides. Note that when this minimal difference ΔT is found between the cold inlet stream and the hot outlet stream, it is denoted "cold end ΔT", while in the reverse case (i.e., when the minimal ΔT is found between the hot inlet stream and the cold outlet stream), it is denoted "hot end ΔT".

Regarding the continuous process variables P_{out} compressor and $T_{cooling}$, optimal values are the same as those obtained when solving the NLP problem at a fixed layout. This result was expected since it was observed previously that the same values of P_{out} and $T_{cooling}$ were obtained regardless of the selected layout.

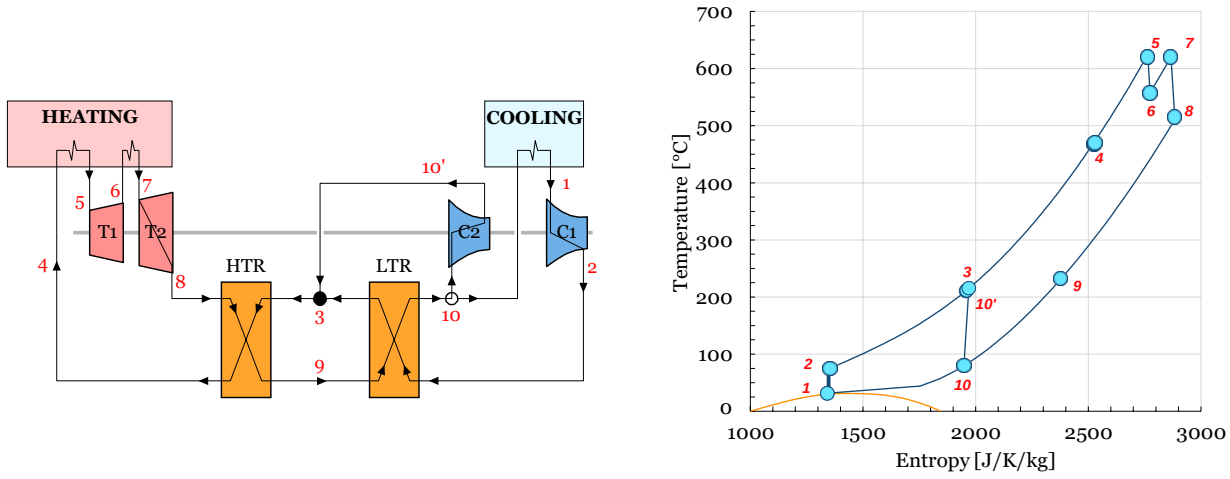

Figure S5: Optimal S-CO_2 Brayton cycle (flowsheet and representation in the T-S plane) based on the optimization of a simplified superstructure.

Table S3: Variability of the results obtained for the simplified superstructure of the S-CO_2 Brayton cycle according to the initial guesses.

Variable Specification	Variable range	Final results obtained from 4 different initial guesses ("seeds")			
		seed=0	seed=1	seed=2	seed=3
Optimization variables					
Switch integer variables y	$y_{1,2,3} \in \{1, 2\}$	{2, 2, 1}	{2, 2, 1}	{2, 2, 1}	{2, 2, 1}
Compressor C1 inlet pressure $P_{C1,in}$ (MPa)	$x_1 \in [3.3 - 10]$	7.50	7.66	7.63	7.57
Cooling S-CO_2 temperature $T_{cooling}$(K)	$x_2 \in [304.35 - 373.15]$	304.35	304.74	304.35	304.39
Recompression flow ratio (%)	$x_3 \in [10^{-6} - 0.5]$	0.34	0.33	0.34	0.34
Compressor C1 outlet pressure $P_{C1,out}$ (MPa)	$x_4 \in [3.3 - 30]$	30.00	30.00	30.00	30.00
Expansion ratio (turbine T1) (-)	$x_6 \in [1 - 5]$	1.92	2.04	1.91	1.99
Cold stream outlet T_{LTR} (K)	$x_5 \in [304.35 - 893.15]$	495.03	503.96	488.12	490.36
Hot stream outlet T_{HTR} (K)	$x_7 \in [304.35 - 893.15]$	504.56	513,.58	497.63	499.94
Constraints					
LTR cold end ΔT (K)	$g_1 = (\Delta T - 10) \geq -0.5$	-0.46	-0.49	-0.41	-0.45
LTR hot end ΔT (K)	$g_2 = (\Delta T - 10) \geq -0.5$	0.00	4.58	0.00	-0.3
HTR hot end ΔT (K)	$g_3 = (\Delta T - 10) \geq -0.5$	35.05	38.29	36.72	36.08
HTR cold end ΔT (K)	$g_4 = (\Delta T - 10) \geq -0.5$	-0.46	-0.41	-0.49	-0.41
Compression ratio C1 (-)	$g_5 = (P_2/P_1 - 1) \geq -0.025$	59.97	58.36	58.60	59.26
Structure nomenclature		1RH-2R-1RC			
Final cycle efficiency (%)		**51.38**	**50.93**	**51.36**	**51.34**

2 Process Flow Diagram of Energy Optimization

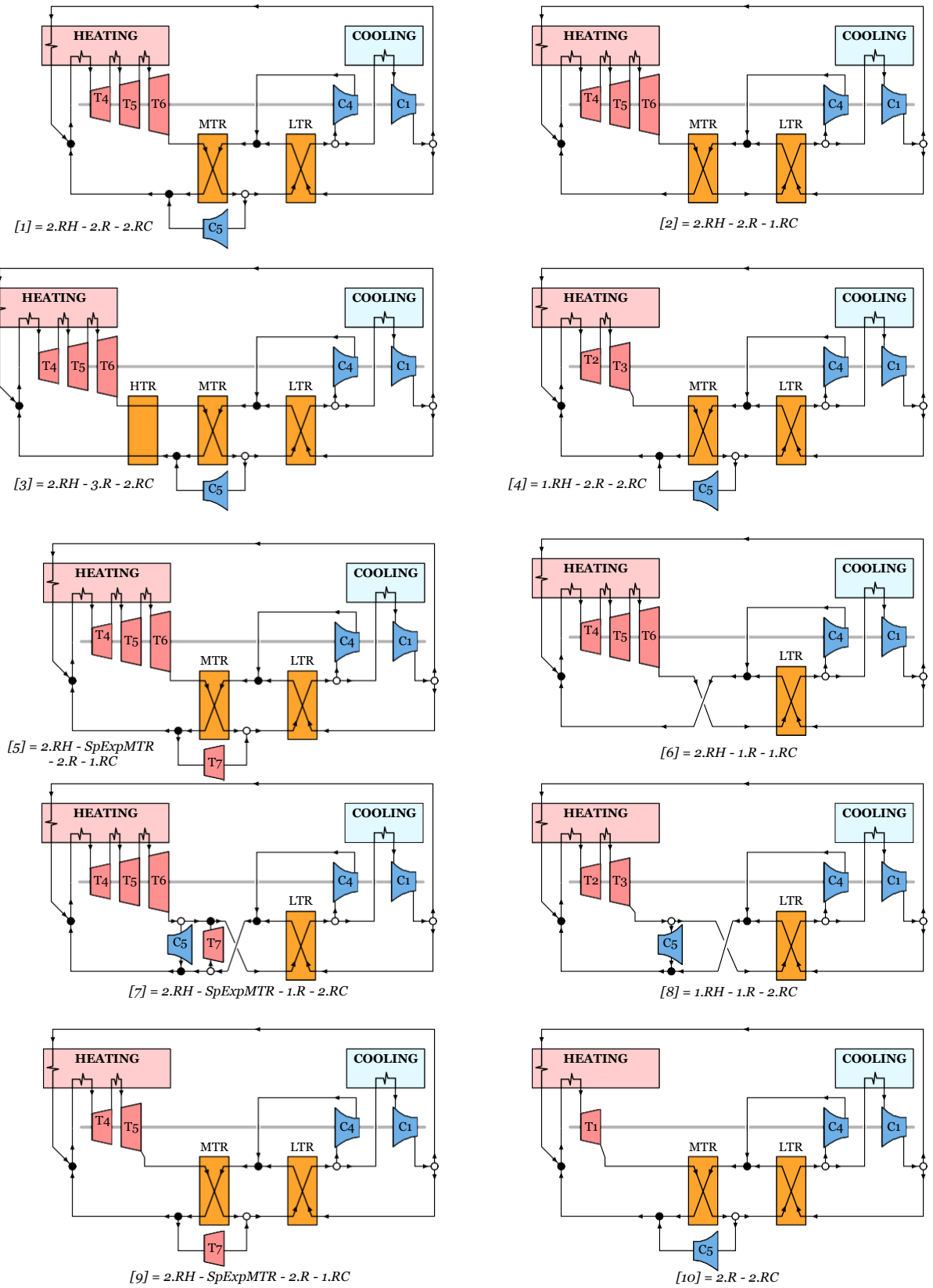

Figure S6: Simplified Process Flow Diagram of the 10 configurations from Table 2 of the main article

References

[1] M. Mecheri and Y. Le Moullec. Supercritical CO_2 Brayton cycles for coal-fired power plants. *Energy*, 103:758–771, 2015.

[2] E.G. Feher. The supercritical thermodynamic power cycle Douglas Paper No.4348. In *Proceedings of the Intersociety Energy Conversion Engineering Conference*, pages 13–17, Miami Beach, August 1967.

[3] G. Angelino. Real gas effects in carbon dioxide cycles. *ASME Paper*, No. 69-GT-103:1–12, 1969.